

# A retractable structure based on Bricard linkages and rotating rings of tetrahedra

Yaozhi Luo \*, Ying Yu, Jingjing Liu

*Space Structures Research Center, Zhejiang University, Hangzhou 310027, China*

Received 11 January 2007; received in revised form 7 July 2007

Available online 8 September 2007

---

## Abstract

Retractable structures which alter their geometries according to practical requirements are widely used in roof structures of stadiums for their versatility. A retractable structure based on threefold-symmetric Bricard linkages and rotating rings of tetrahedra is proposed and developed in this paper. By replacing each link of a threefold-symmetric Bricard linkage with a tetrahedron, a retractable structure is obtained which can repeatedly open and close by rotating the tetrahedra. The geometric relationship between the retractable structure and the threefold-symmetric Bricard linkage is derived and ranges of main geometric parameters are determined to ensure a continuous and smooth movement in the deployment of the structure. Then the relative displacement of the support and the open rate of the structure, two main parameters concerned in practical applications, are investigated. Preferred ranges of main geometric parameters are proposed and a physical model is manufactured to verify them. A discussion on some possible improvements and modifications of the structure is also presented.

© 2007 Elsevier Ltd. All rights reserved.

**Keywords:** Mechanism; Bricard linkage; Ring of tetrahedra; Retractable structure; Deploying performance

---

## 1. Introduction

Gan and Pellegrino (2003) have suggested 3D mechanisms used for deployable structures in space technology. The deployment of these structures depends on the movement of mechanisms. This deployment can be repeated without inducing any strain in structural components. Overconstrained mechanisms such as the Bennett linkage and the Bricard linkage are preferred in deployable structure (Chen and You, 2005; Chen et al., 2005), because extra stiffness is provided.

In this paper, we develop a retractable structure based on the Bricard linkage. This kind of linkage, which includes three different types of mobile octahedra (Bricard, 1897) and three additional types of mobile linkages

---

\* Corresponding author. Tel./fax: +86 571 87952349.

E-mail address: [Luoyz@zju.edu.cn](mailto:Luoyz@zju.edu.cn) (Y. Luo).

**Notation**

$R_i$	offset between endpoints of two links connected by one revolute joint along the axis $i$
$S_c$	projection area of a tetrahedron onto the horizontal plane in fully closed configuration
$\Delta S$	projection area of the central open part of a tetrahedron onto the horizontal plane in the configuration during the process of deployment
$U_o$	distance between the support and the central axis of the structure in the configuration during the process of deployment
$U_c$	distance between the support and the central axis of the structure in fully closed configuration
$\Delta U$	displacement of the support in the configuration during the process of deployment
$W_o$	distance between the top-point of the roof-axis and the central axis of the structure in the configuration during the process of deployment
$a$	projection edge length of the hexagonal roof in fully closed configuration
$c$	height of the fully closed roof
$d$	length of support-axes
$l$	length of links of a Bricard linkage
$\alpha$	twist angle between axes of adjacent revolute joints of a Bricard linkage
$\lambda_s$	open rate of the structure
$\lambda_U$	relative displacement of the support
$\tau(\gamma)$	slope angle of the support-axis (the roof-axis)
$\tau_c(\gamma_c)$	value of $\tau(\gamma)$ when the structure is fully closed ( $\gamma_c = \arctan(\xi)$ )
$\tau_o(\gamma_o)$	value of $\tau(\gamma)$ when the structure is fully open
$\xi$	$c/a$
$\eta$	$d/a$

(Bricard, 1927), is the most remarkable six-bar overconstrained mechanism with revolute joints. And it is the only six-bar, revolute joints, closed-loop overconstrained mechanisms that is independent of four-bar and five-bar mechanisms. Baker (1980) made a thorough analysis of all the six Bricard linkages by appropriately setting independent closure equations. Recently, Chen et al. (2005) presented a kinematic analysis of a new linkage called threefold-symmetric Bricard linkage and pointed out the possibility of applying this linkage in deployable structures.

The ring of tetrahedra is well known in the field of toys making and its associated mathematics problems. It is a rotating ring made of identical tetrahedra which are connected by shared edges acting like hinges. Stalker (1933) described the motion of certain members of rotating rings of tetrahedra as ‘amusing and confusing’, like a smoke ring. Fowler and Guest (2000) found a symmetry extension of Maxwell’s rule for rigidity of frames which strengthened the original one. Later, they studied rings of  $N$  tetrahedra by those symmetry-adapted versions of classical counting rules of mechanism analysis, and provided a general analysis of the mechanisms and states of self-stress in this subset of rotating rings of tetrahedra (Fowler and Guest, 2005). The ring of six tetrahedra has three planes of symmetry in each position (condition 1) and the two connecting edges of each tetrahedron are perpendicular to each other (condition 2). If only condition 1 is considered, the ring is still rotatable (Chen et al., 2005). Thus, if the six links of a threefold-symmetric Bricard linkage are substituted with six tetrahedra, the structure is still mobile, which ensures the existence of the new retractable structure.

The purpose of this paper is to investigate the geometric and kinematic characteristics of the above-mentioned retractable structure. The layout of this paper is as follows. First, the general configuration of the structure is given in Section 2. Then Section 3 derives the relationship between the structure and its corresponding threefold-symmetric Bricard linkage. The deploying performance of the structure is investigated in Section 4. At last, achievements up to now are concluded, and some possible configurations of the retractable structure are discussed.

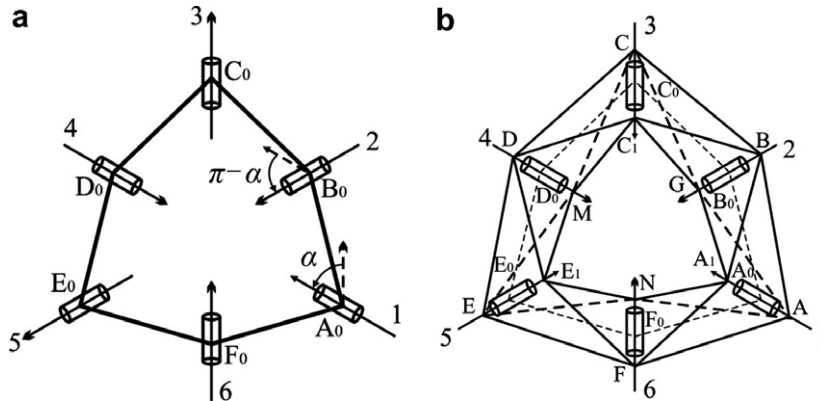


Fig. 1. (a) Threefold-symmetric Bricard linkage; (b) the retractable structure.

## 2. Geometric configuration of the retractable roof

The threefold-symmetric Bricard linkage satisfies the following conditions:

$$\begin{cases} l_{12} = l_{23} = l_{34} = l_{45} = l_{56} = l_{61} = l, \\ \alpha_{12} = \alpha_{34} = \alpha_{56} = \alpha, \quad \alpha_{23} = \alpha_{45} = \alpha_{61} = 2\pi - \alpha, \\ R_i = 0 \quad (i = 1, 2, 3, 4, 5, 6), \end{cases} \quad (1)$$

where  $l_{jk}$  is the length of a link between two adjacent axes of revolute joints  $j$  and  $k$ ,  $\alpha_{jk}$  is the twist angle between axes of adjacent revolute joints  $j$  and  $k$  ( $j, k = 1, 2, 3, 4, 5, 6$ ), and  $R_i$  is the offset between endpoints of two links connected by one revolute joint along the axis  $i$ .

The configuration of this linkage is shown in Fig. 1(a). It has three planes of symmetry and also threefold-rotational symmetry. Each link of the linkage is perpendicular to the two axes of adjacent revolute joints it connects. By substituting the links with tetrahedra, a deployable structure is obtained, shown in Fig. 1(b). The revolute joints of the threefold-symmetric Bricard linkage become the connecting edges ( $AA_1$ ,  $BG$ ,  $CC_1$ ,  $DM$ ,  $EE_1$  and  $FN$ ) of the structure, while each link ( $A_0B_0$ ,  $B_0C_0$ ,  $C_0D_0$ ,  $D_0E_0$ ,  $E_0F_0$  and  $F_0A_0$ ) is perpendicular to both connecting edges of the corresponding tetrahedron. Any two adjacent tetrahedra are chiral versions of each other.

Two different configurations of the retractable structure are shown in Figs. 2 and 3. According to their positions in the structure, three of the six connecting edges ( $AA_1$ ,  $CC_1$ , and  $EE_1$ ) are called roof-axis, and the other three ( $BG$ ,  $DM$  and  $FN$ ) called support-axis (Fig. 2). Supports ( $G$ ,  $M$  and  $N$ ) of the structure are located at the bottom of the support-axes. If roof-axes and support-axes are extended,  $AA_1$ ,  $CC_1$ , and  $EE_1$  will meet at point  $O_1$ , and  $BG$ ,  $DM$  and  $FN$  at point  $O_2$ .  $O_1O_2$  intersects the plane  $A_0C_0E_0$  and  $B_0D_0F_0$  at points  $O_{01}$  and  $O_{02}$ , respectively. Both the plane  $A_0C_0E_0$  and  $B_0D_0F_0$  are parallel to the horizontal plane. In Fig. 3, roof-axes meet at point  $O$ .  $A$ ,  $B$ ,  $C$ ,  $D$ ,  $E$  and  $F$  are coplanar and  $O'$  is the center of the hexagon  $ABCDEF$ .

When the supports move towards the central axis ( $O_1O_2$  in Fig. 2 or  $O'O$  in Fig. 3) of the structure, the roof opens gradually, turning outwards like a flower. On the contrary, when the supports move away from the central axis, the roof closes gradually. And it is fully closed as contact occurs between the inner-faces of tetrahedra.

## 3. Relationship between the structure and the threefold-symmetric Bricard linkage

The geometric relationship between the structure and the corresponding threefold-symmetric Bricard linkage is derived in this section. In practice, it is not necessary to know the characteristics of the original linkage. The design work can be done based on the design parameters of the retractable structure  $a$ ,  $\tau$ ,  $\xi$  and  $\eta$ , where  $a$  is the projection edge length of the hexagonal roof in fully closed configuration,  $\tau$  is the slope angle of the support-axis,  $\xi$  is equal to  $c/a$ ,  $\eta$  is equal to  $d/a$ , and  $c$  is the length of support-axes,  $d$  is the height of the fully

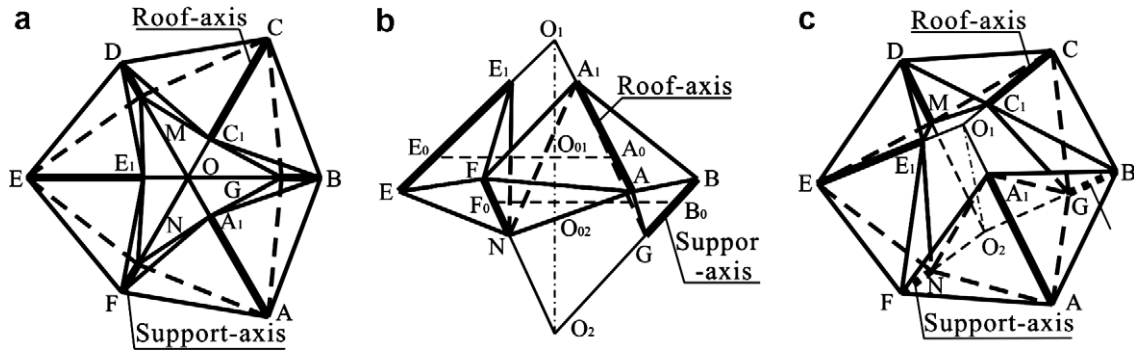


Fig. 2. Retractable structure in the configuration during the process of deployment. (a) Plan view; (b) elevation view; (c) axonometric view.

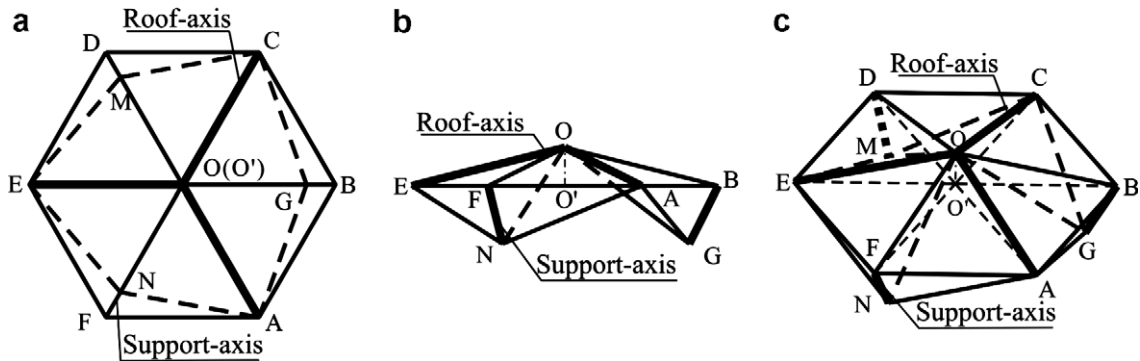


Fig. 3. Retractable structure in fully closed configuration. (a) Plan view; (b) elevation view; (c) axonometric view.

closed roof. However, some important features of the structure can be summarized from the relationship, which are very helpful for the investigation of the deploying performance of the structure in Section 4.

Because of symmetry, only one tetrahedron  $A_1ABG$  is considered in detail. Fig. 4(a) shows the tetrahedron in fully closed configuration. Left-handed Cartesian coordinate system  $O'XYZ$  is adopted here, setting  $O'$  as original point,  $O'B$  as X-axis,  $O'Q$  ( $Q$  is the mid-point of  $AF$ ) as Y-axis and  $O'O$  as Z-axis.  $A_0B_0$  perpendicularly intersects  $A_1A$  and  $BG$  at  $A_0$  and  $B_0$ , respectively. Denote the length of  $A_1A_0$  as  $e$ ,  $A_0A$  as  $f$  and  $B_0B$  as  $h$ . From Appendix A, we have

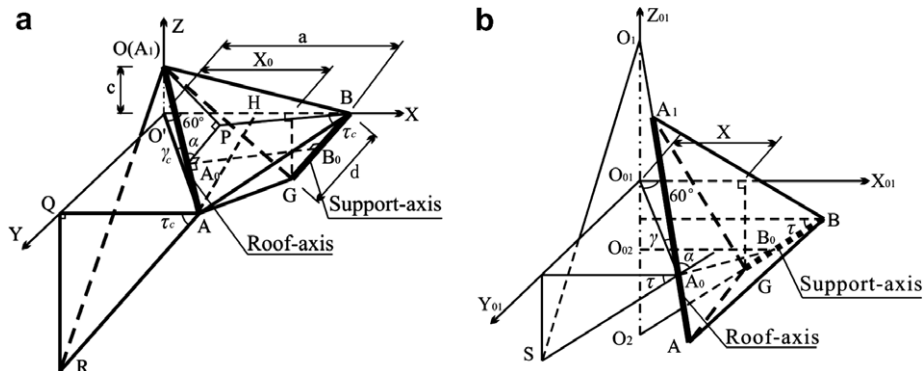


Fig. 4. Tetrahedron  $A_1ABG$ . (a) The fully closed configuration; (b) the configuration during the process of deployment.

$$l = \frac{\sqrt{3} \cdot (\sin \tau_c + \xi \cos \tau_c)}{\sqrt{(4\xi^2 - 1) \cos^2 \tau_c + 4 + 4\xi \sin \tau_c \cos \tau_c}} \cdot a \quad (2)$$

$$\begin{cases} e = \frac{2(2+3\xi^2) - 2(2-\xi^2-4\xi^4) \cos^2 \tau_c + 12\xi(1+\xi^2) \sin \tau_c \cos \tau_c}{2\sqrt{1+\xi^2[(4\xi^2-1) \cos^2 \tau_c + 4 + 4\xi \sin \tau_c \cos \tau_c]}} \cdot a, \\ f = \frac{2(2+\xi^2) + 2(1+2\xi^2) \cos^2 \tau_c - 4\xi(1+\xi^2) \sin \tau_c \cos \tau_c}{2\sqrt{1+\xi^2[(4\xi^2-1) \cos^2 \tau_c + 4 + 4\xi \sin \tau_c \cos \tau_c]}} \cdot a, \\ h = \frac{(3+2\xi^2) \cos \tau_c - 2\xi \sin \tau_c}{4 + (4\xi^2-1) \cos^2 \tau_c + 4\xi \sin \tau_c \cos \tau_c} \cdot a. \end{cases} \quad (3)$$

Fig. 4(b) shows the tetrahedron  $A_1ABG$  in the configuration during the process of deployment. If the original point of coordinate system  $O'XYZ$  is moved to point  $O_{01}$ , a new coordinate system  $O_{01}X_{01}Y_{01}Z_{01}$  is obtained.  $A_0S$  is parallel to  $B_0B$  and intersects the plane  $O_{01}Y_{01}Z_{01}$  at  $S$ . By using the law of cosines in  $\Delta O_1A_0S$ , we can obtain that

$$\cos(\alpha) = \sin \gamma \sin \tau - \frac{1}{2} \cos \gamma \cos \tau. \quad (4)$$

So Eqs. (2)–(4) relate design parameters of the retractable structure to geometric parameters of the threefold-symmetric Bricard linkage. As a result, once given a retractable structure, the corresponding Bricard linkage can be determined.

Following the naming in (Chen et al., 2005), (4) is called input–output equation and the curve determined by it called compatibility path. It is obvious that the equation is periodic and the period is  $360^\circ$  for both  $\tau$  and  $\gamma$ . According to (4), one of slope angles  $\tau$  or  $\gamma$  can be free for any given  $\alpha$ . Thus, same as the threefold-symmetric Bricard linkage, the retractable structure has a single DOF, regardless of kinematic bifurcation points.

Fig. 5 can reflect some characteristics of the structure. Firstly, when the structure is opening,  $\tau$  is decreasing while  $\gamma$  is increasing, which also can be found in physical models we made. Secondly, in one period of the curve, the compatibility paths are discontinuous when  $0^\circ \leq \alpha < 60^\circ$  and  $120^\circ < \alpha \leq 180^\circ$ . In general, they are two closed loops in space interval I and III, and in II and IV, respectively. In some particular situations ( $\alpha = 0^\circ$  or  $180^\circ$ ), they are just two points. Because of physical blocked,  $\tau$  or  $\gamma$  cannot pass through one close loop to the other. So the structure moves discontinuously in these two ranges. On the contrary, when  $60^\circ < \alpha < 120^\circ$ , the compatibility paths are continuous in space interval I and III, and in II and IV, respectively. Therefore, the structure can move continuously within this range. Thirdly, for  $\alpha = 60^\circ$  or  $120^\circ$ , the bifurcation of the compatibility paths appears. Take the case when  $\alpha = 120^\circ$  as an example, assuming that the structure moves along the path C120a, when it reaches point K where  $\tau = 0^\circ$  and  $\gamma = 0^\circ$ , there are two

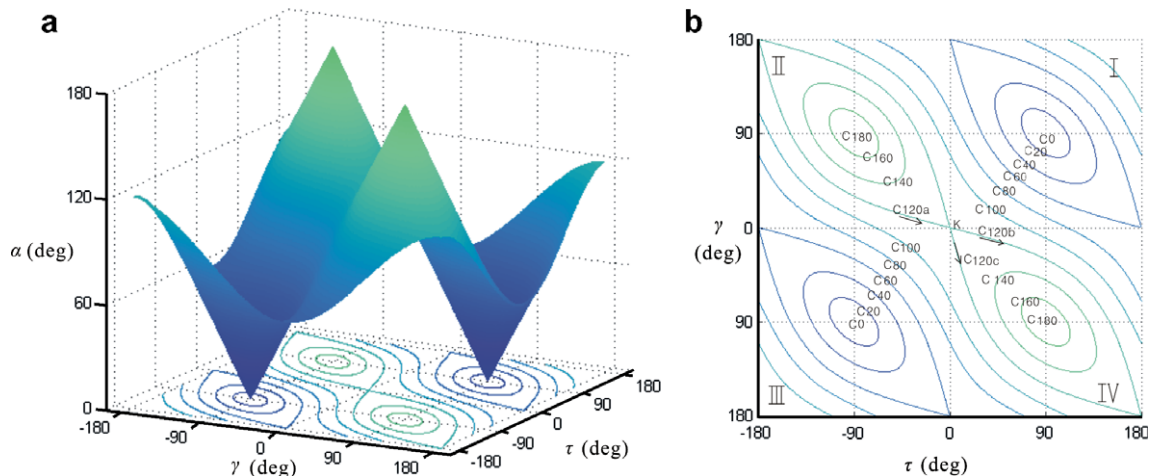


Fig. 5. (a)  $\tau$  vs.  $\gamma$  as a function of  $\alpha$  for the structure in a period. The  $\alpha$ -contours are spaced at  $20^\circ$ ; (b) the  $\alpha$ -contours in detail. “Cx” means the  $\alpha$ -contour when  $\alpha = x^\circ$ .

possible compatibility paths (C120b and C120c) of the structure. In other words, the compatibility path cannot be uniquely determined at the point K.

In conclusion, it is better to choose suitable pairs of  $\tau$  and  $\gamma$  to ensure that the value of  $\alpha$  is in the range of  $60^\circ < \alpha < 120^\circ$ , thus the structure can have continuous and uniquely determined movement.

#### 4. Deploying performance of the retractable structure

When the structure moves, attention is focused on its deploying performance. In this section, two main parameters concerned in practical applications, the relative displacement of the support  $\lambda_U$  and the open rate of the structure  $\lambda_s$ , are chosen to be investigated to reflect the structure's deploying performance. The case when  $\xi = 0.25$  and  $\eta = 0.2$  is considered here. Following the suggestion at the end of Section 3, when  $-3.8^\circ < \tau_c < 130.7^\circ$ , the value of  $\alpha$  is in the desirable range and the structure can have uniquely determined and continuous kinematic path.

Since  $\Delta U$  is the displacement of the support, and  $\Delta S$  is the projection area of the central open part during the process of deployment,  $\Delta U/a$  ( $\lambda_U$ ) and  $\Delta S/S_c$  ( $\lambda_s$ ) will not be influenced by the dimension of the structure. A detailed derivation is given in Appendix B from which we can obtain the following expressions,

$$\lambda_U = \frac{\Delta U}{a} = 1 - \eta \cos \tau_c + \frac{\sqrt{3}(d-h) \sin \alpha \cos \tau - (2 \sin \tau \cos \gamma + \cos \tau \sin \gamma) \cdot l}{\sqrt{3}a \sin \alpha}, \quad (5)$$

$$\lambda_s = \frac{\Delta S}{S_c} = \left[ \frac{(2 \sin \tau \cos \gamma + \cos \tau \sin \gamma)}{\sqrt{3}a^2 \sin \alpha} l + \frac{(h-d) \cos \tau}{a^2} \right] \left[ \frac{(\sin \tau \cos \gamma + 2 \cos \tau \sin \gamma)}{\sqrt{3}a^2 \sin \alpha} l - \frac{e \cos \gamma}{a^2} \right]. \quad (6)$$

Fig. 6 shows the variations of  $\lambda_U$  in the deploying process of the structure. It is apparent that  $\lambda_U$  first increases from  $\lambda_U = 0$ , and it begins to decrease after passing through the point  $\tau = 0$ . The two cases,  $\lambda_U = 0$  and  $\lambda_U = 1$ , indicate two extreme states of the structure. When  $\lambda_U = 0$ , the structure is fully closed. When  $\lambda_U = 1$ , supports G, M and N meet at one point, which only appears in the situation of  $\tau_c \geq 95.4^\circ$ .  $\lambda_U > 1$  also appears in Fig. 6, but it is meaningless because the tetrahedra are considered as rigid bodies. Hence, when  $\tau_c \geq 95.4^\circ$ , we should limit the range of  $\tau_o$  to avoid the meaningless part of  $\lambda_U$ . For example, when  $-35.5^\circ < \tau < 35.5^\circ$ , the value of  $\lambda_U$  is larger than 1 for the structure that  $\tau_c = 110^\circ$ ,  $\xi = 0.25$  and  $\eta = 0.2$ , so we set  $\tau_o = 35.5^\circ$  for this structure. When  $\tau_c < 95.4^\circ$ , theoretically  $\tau_o$  can be any value smaller than  $\tau_c$ , but

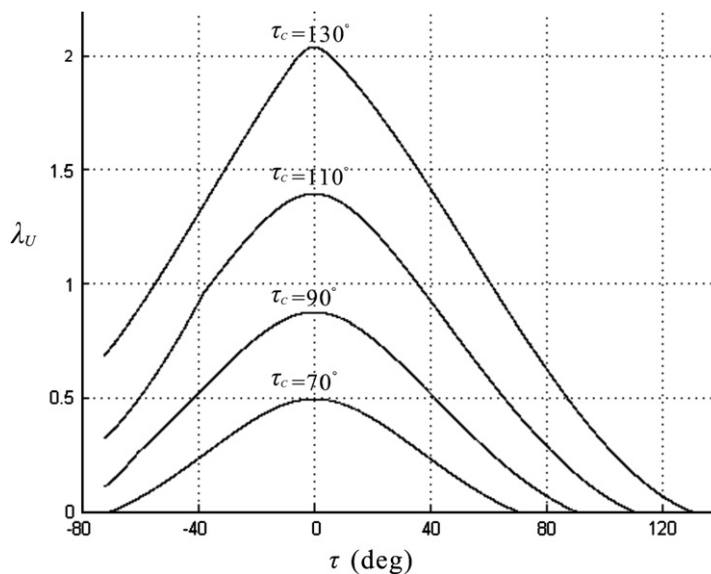


Fig. 6.  $\lambda_U$  vs.  $\tau$  for a set of  $\tau_c$  when  $\xi = 0.25$  and  $\eta = 0.2$ .



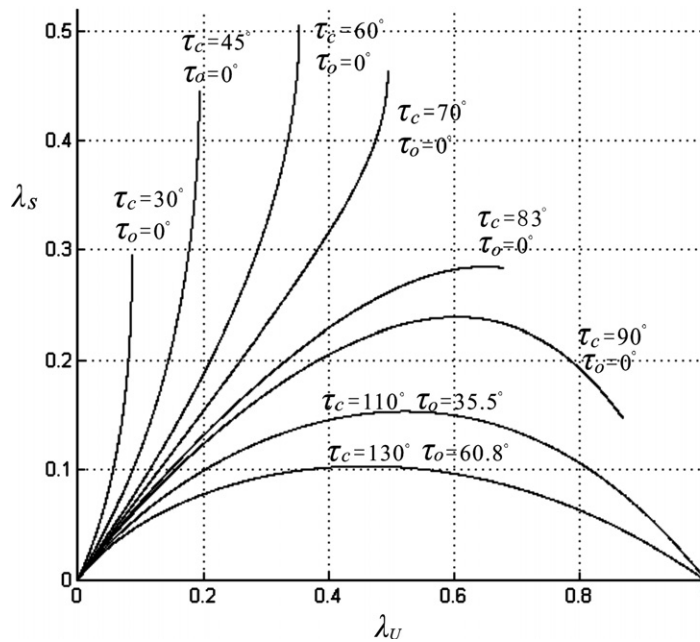


Fig. 7.  $\lambda_s$  vs.  $\lambda_U$  for a set of  $\tau_c$  when  $\xi = 0.25$  and  $\eta = 0.2$ .

actually it is hard to control the deployment in a practical structure if the supports change their movement direction in the deploying process. Thus, we set  $\tau_o = 0^\circ$ .

The relationship between  $\lambda_U$  and  $\lambda_s$  is shown in Fig. 7. When  $\tau_c > 83^\circ$  (case 1),  $\lambda_s$  first increases and then decreases in the deploying process of the structure. Note that both curves representing  $\tau_c = 110^\circ$  and  $\tau_c = 130^\circ$ , pass through the point (1,0), which means that the structure is fully closed again at last. This phenomenon is shown in Fig. 8(a). When  $\tau_c < 83^\circ$  (case 2),  $\lambda_s$  rises all the time and a smaller  $\tau_c$  corresponds to a larger  $\lambda_s$  under a settled  $\lambda_U$ . Each maximum of  $\lambda_s$  in this case is bigger than it in case 1, which brings a larger central open part of the structure. The deploying way of the structure in case 2 is shown in Fig. 8(b).

Obviously, structures with  $\tau_c < 83^\circ$  are preferred in practical application. A physical model is made to verify the above conclusion, as shown in Fig. 9. In this case, it should be pointed out that the tangent of the curves

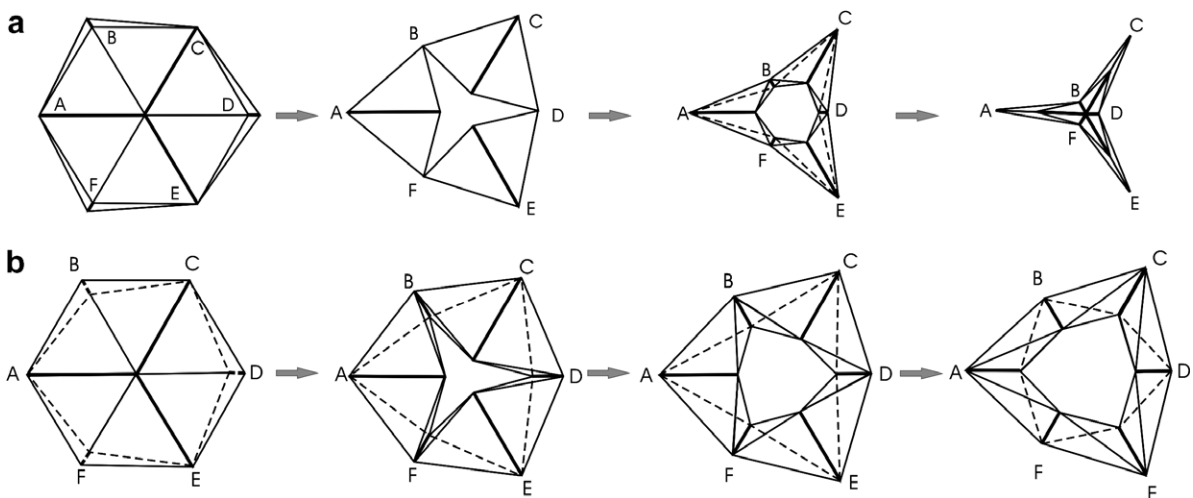


Fig. 8. Different deploying way (a) when  $\tau_c > 83^\circ$  and (b) when  $\tau_c < 83^\circ$ .

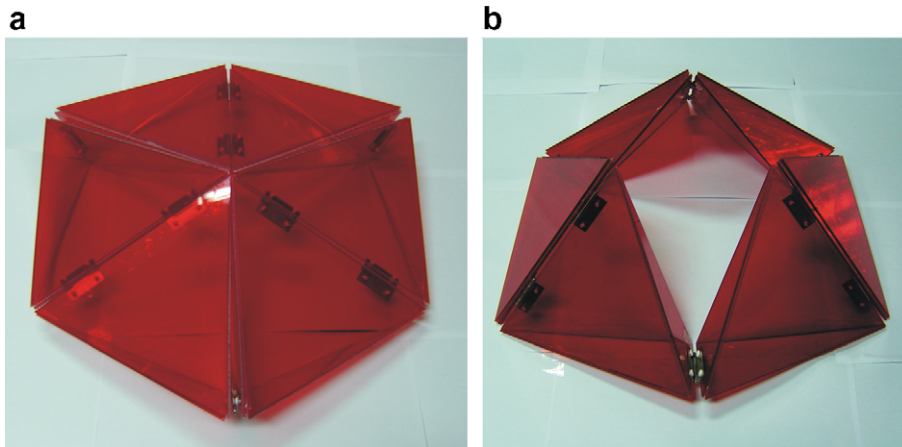


Fig. 9. A retractable structure model that  $a=210$  mm,  $\xi = 0.25$ ,  $\eta = 0.2$  and  $\tau_c = 45^\circ$ . (a) The fully closed configuration; (b) the fully open configuration.

increases rapidly, indicating that the increment of the open rate corresponding to a given increment of the support displacement becomes larger in the deploying process. At the end of the process, the tangent tends to be divergent, i.e., a very small  $\lambda_U$  corresponding to a big increment of  $\lambda_s$ , which will bring some dynamic affects to the structure and the movement of the structure is difficult to control at this moment.

## 5. Discussions

The new retractable structure presented in this paper is based on three-symmetric Bricard linkages and rotating rings of tetrahedra. This paper has established the relationship between them and suggested suitable  $\tau$  and  $\gamma$  so the structure can move continuously. The deploying performance of this structure has been analyzed under given  $\xi$  and  $\eta$ . Structures with  $\tau_c < 83^\circ$  is preferred in practical application. The correctness of the theoretical analysis has been verified by the physical model.

Finally, some possible improvements and modifications of the structure are discussed here. Firstly, if the tetrahedra are replaced by pentahedra, the retractable roof (Fig. 10) is still feasible. It is found that the displacement and stress in the new model is much smaller than those in the original one, and the stress concentration on roof axes disappears. Secondly, by changing the number and configuration of tetrahedra, some different retractable roofs (Fig. 11) are obtained. It should be pointed out that when the number of tetrahedra

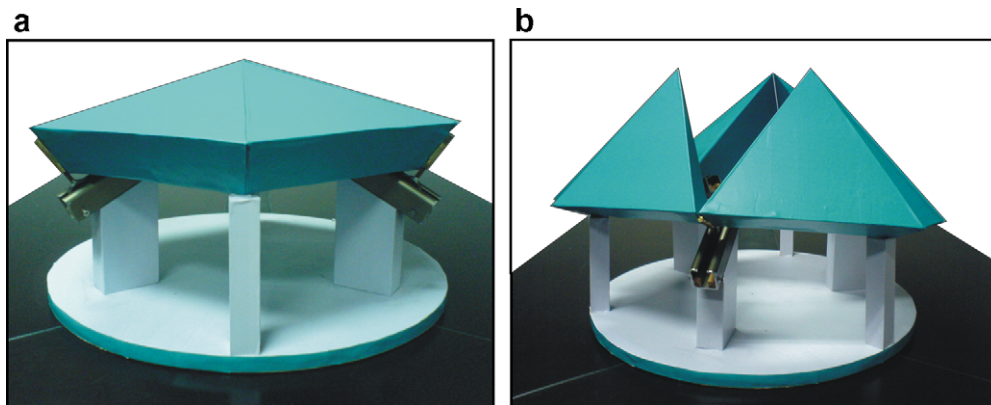


Fig. 10. Retractable structure model that replacing the tetrahedra by pentahedra. (a) The fully closed configuration; (b) the fully open configuration.





Fig. 11. Various configurations of the retractable structure, whose projections onto the horizontal plane is (a) triangle; (b) square; (c) octagon.

is more than six, the retractable structures are not based on the Bricard linkage but other types of mechanisms with more than one DOF.

### Acknowledgements

The project is supported by the National Natural Science Foundation of China (50638050) and NCET-06-0517. The authors are grateful to Dr. Zhong You of Oxford University and Professor Tibor Tarnai of Budapest University of Technology and Economics for their valuable advice and suggestions during the preparation of this work. Luo would like to thank the Y.C. Tang Disciplinary Development Foundation for Senior Visiting Scholar Studying Abroad.

### Appendix A

The basic design parameters of the structure are  $a$ ,  $\xi$ ,  $\tau$  and  $\eta$ . In Fig. 4(a), the edge lengths of the tetrahedron  $A_1ABG$  can be expressed as follows:

$$\begin{cases} \overline{AB} = a, & \overline{BG} = \eta a, & \overline{A_1A} = \overline{A_1B} = a\sqrt{1 + \xi^2}, \\ \overline{A_1G} = a\sqrt{1 + \xi^2 + \eta^2 - 2\eta(\cos \tau_c - \xi \sin \tau_c)}, \\ \overline{AG} = a\sqrt{1 + \eta^2 - \eta \cos \tau_c}. \end{cases} \quad (\text{A.1})$$

$AR$  is parallel to  $BG$  and intersects the plane  $O'YZ$  at  $R$ ;  $A_0P$  is parallel and equal to  $B_0B$ ;  $H$  is the mid-point of  $O'B$  and  $AH$  is perpendicular to plane  $OBG$ . By using the law of cosines in  $\Delta A_1AR$ , we can obtain

$$\cos \alpha = \frac{2\xi \sin \tau_c - \cos \tau_c}{2\sqrt{1 + \xi^2}}. \quad (\text{A.2})$$

The volume of tetrahedron  $A_1ABG$  is

$$V = \frac{1}{6} \overline{A_1A} \cdot \overline{BG} \cdot l \cdot \sin \alpha, \quad (\text{A.3})$$

and it also can be expressed as

$$V = \frac{1}{6} \overline{AH} \cdot \overline{BG} \cdot \overline{A_1B} \cdot \sin \angle A_1BG. \quad (\text{A.4})$$

Considering (A.3) and (A.4), there is

$$l = \frac{\sqrt{3}a \cdot (\sin \tau_c + \xi \cos \tau_c)}{2\sqrt{1 + \xi^2} \sin \alpha}. \quad (\text{A.5})$$

Substituting (A.2) into (A.5) yields

$$l = \frac{\sqrt{3} \cdot (\sin \tau_c + \xi \cos \tau_c)}{\sqrt{(4\xi^2 - 1) \cos^2 \tau_c + 4 + 4\xi \sin \tau_c \cos \tau_c}} \cdot a. \quad (2)$$

In  $\Delta A_1AB$ , we have

$$\begin{cases} \overline{A_1B} = \sqrt{l^2 + e^2 + h^2 - 2eh \cos \alpha} = a\sqrt{1 + \xi^2}, \\ \overline{AB} = \sqrt{l^2 + f^2 + h^2 + 2fh \cos \alpha} = a, \\ \overline{A_1A} = e + f = a\sqrt{1 + \xi^2}. \end{cases} \quad (\text{A.6})$$

Considering (A.2), the solution to (A.6) can be expressed as

$$\begin{cases} e = \frac{2(2+3\xi^2) - 2(2-\xi^2-4\xi^4) \cos^2 \tau_c + 12\xi(1+\xi^2) \sin \tau_c \cos \tau_c}{2\sqrt{1+\xi^2}[(4\xi^2-1) \cos^2 \tau_c + 4+4\xi \sin \tau_c \cos \tau_c]} \cdot a, \\ f = \frac{2(2+\xi^2) + 2(1+2\xi^2) \cos^2 \tau_c - 4\xi(1+\xi^2) \sin \tau_c \cos \tau_c}{2\sqrt{1+\xi^2}[(4\xi^2-1) \cos^2 \tau_c + 4+4\xi \sin \tau_c \cos \tau_c]} \cdot a, \\ h = \frac{(3+2\xi^2) \cos \tau_c - 2\xi \sin \tau_c}{4+(4\xi^2-1) \cos^2 \tau_c + 4\xi \sin \tau_c \cos \tau_c} \cdot a. \end{cases} \quad (3)$$

## Appendix B

In Fig. 2, edge lengths of  $\Delta A_0C_0E_0$  and  $\Delta B_0D_0F_0$  are denoted as  $a_0$  and  $b_0$ , respectively.  $O_{01}O_{02}$  is the distance between plane  $A_0C_0E_0$  and plane  $B_0D_0F_0$ , denoted as  $c_0$ . So

$$\begin{cases} \tan \tau = (\frac{\sqrt{3}}{3}b_0 - \frac{\sqrt{3}}{6}a_0)/c_0, \\ \tan \gamma = (\frac{\sqrt{3}}{3}a_0 - \frac{\sqrt{3}}{6}b_0)/c_0, \\ l = \sqrt{(a_0^2 - a_0b_0 + b_0^2)/3 + c_0^2}. \end{cases} \quad (\text{B.1})$$

Considering (A.2), the solution to (B.1) can be expressed as

$$\begin{cases} a_0 = \frac{(\sin \tau \cos \gamma + 2 \cos \tau \sin \gamma)}{\sin \alpha} l, \\ b_0 = \frac{(2 \sin \tau \cos \gamma + \cos \tau \sin \gamma)}{\sin \alpha} l, \\ c_0 = \frac{\sqrt{3}l}{2\sqrt{(\tan^2 \tau + \tan \tau \tan \gamma + \tan^2 \gamma) + 3/4}}. \end{cases} \quad (\text{B.2})$$

In Fig. 2, the distance between the support-point G and central axis  $O_1O_2$  is

$$U_o = \frac{b_0}{\sqrt{3}} - (d - h) \cos \tau = \frac{(2 \sin \tau \cos \gamma + \cos \tau \sin \gamma)l - \sqrt{3}(d - h) \sin \alpha \cos \tau}{\sqrt{3} \sin \alpha}. \quad (\text{B.3})$$

The distance between the top-point  $A_1$  and the central axis  $O_1O_2$  is

$$W_o = \frac{a_0}{\sqrt{3}} - e \cos \gamma = \frac{(\sin \tau \cos \gamma + 2 \cos \tau \sin \gamma) \cdot l - \sqrt{3}e \cos \gamma \sin \alpha}{\sqrt{3} \sin \alpha}, \quad (\text{B.4})$$

and the projection area of the central open part  $\Delta OA_1G$  is

$$\Delta S = \frac{1}{2} U_o W_o \sin 60^\circ. \quad (\text{B.5})$$

In Fig. 3, the distance between the support-point G and central axis  $O_1O_2$  is

$$U_c = a - d \cos \tau_c, \quad (\text{B.6})$$

and the projection area of  $\Delta A_1AB$  is

$$S_c = \frac{1}{2} a^2 \sin 60^\circ. \quad (\text{B.7})$$

So the displacement of supports during the process of deployment is

$$\Delta U = U_c - U_o = a - d \cos \tau_c + \frac{\sqrt{3}(d-h) \sin \alpha \cos \tau - (2 \sin \tau \cos \gamma + \cos \tau \sin \gamma) \cdot l}{\sqrt{3} \sin \alpha}, \quad (\text{B.8})$$

and the relative displacement of the support is

$$\lambda_U = \frac{\Delta U}{a} = 1 - \eta \cos \tau_c + \frac{\sqrt{3}(d-h) \sin \alpha \cos \tau - (2 \sin \tau \cos \gamma + \cos \tau \sin \gamma) \cdot l}{\sqrt{3} a \sin \alpha}. \quad (5)$$

The open rate of the structure is

$$\lambda_s = \frac{\Delta S}{S_c} = \left[ \frac{(2 \sin \tau \cos \gamma + \cos \tau \sin \gamma)}{\sqrt{3} a^2 \sin \alpha} l + \frac{(h-d) \cos \tau}{a^2} \right] \left[ \frac{(\sin \tau \cos \gamma + 2 \cos \tau \sin \gamma)}{\sqrt{3} a^2 \sin \alpha} l - \frac{e \cos \gamma}{a^2} \right]. \quad (6)$$

## References

- Baker, J.E., 1980. An analysis of Bricard linkages. *Mechanism and Machine Theory* 15, 267–286.
- Bricard, R., 1897. Mémoire sur la théorie de l'octaédre articulé. *Journal de mathématiques pures et appliquées*, Liouville 3, 113–148.
- Bricard, R., 1927. In: *Leçons de cinématique*, vol. 2. Springer, USA, pp. 7–12.
- Chen, Y., You, Z., 2005. Mobile assemblies based on the Bennett linkage. *Proceedings of the Royal Society of London Series A* 461, 1229–1245.
- Chen, Y., You, Z., Tarnai, T., 2005. Threefold-symmetric Bricard linkages for deployable structures. *International Journal of Solids and Structures* 42, 2287–2301.
- Fowler, P.W., Guest, S.D., 2000. A symmetry extension of Maxwell's rule for rigidity of frames. *International Journal of Solids and Structures* 37, 1793–1804.
- Fowler, P.W., Guest, S.D., 2005. A symmetry analysis of mechanisms in rotating rings of tetrahedra. *Proceedings of the Royal Society: Mathematical, Physical & Engineering Science* 461 (2058), 1829–1846.
- Gan, W.W., Pellegrino, S., 2003. Closed-Loop Deployable Structures, AIAA 2003-1450. In: *Proceeding of 44th AIAA/ASME/ASCE/AHS/ASC structures, Structural Dynamics and Materials Conference*, Norfolk, April 7–10 2003.
- Stalker, R.M., 1933. Advertising medium or toy. US Patent 1,997,022, filed April 27, 1933, and issued April 9, 1935.